The FENE-L and FENE-LS closure approximations to the kinetic theory of finitely extensible dumbbells*

G. Lielens, R. Keunings, V. Legat
CESAME, Division of Applied Mechanics,
Université catholique de Louvain, Bâtiment Euler,
B-1348 Louvain-la-Neuve, Belgium

April 12, 1999

Abstract

We address the closure problem for the Warner Finitely Extensible Non-Linear Elastic (FENE) dumbbell model of a dilute polymer solution. The FENE-L closure model, introduced recently for one-dimensional elongational flows (Lielens *et al.* J. Non-Newtonian Fluid Mech. 76 (1998) 249-279), is extended to general flow kinematics. A simplified version of the theory, referred to as the FENE-LS model, is also proposed. Simulations of steady-state and transient rheometrical flows reveal the superiority of the FENE-L and FENE-LS constitutive equations with respect to the simpler FENE-P closure in describing the rheological response of the FENE kinetic theory.

Keywords: Constitutive equation; closure approximation; FENE dumbbells; kinetic theory

1 Introduction

In a recent paper [1], we proposed a general framework for addressing the closure problem in the kinetic theory of flowing polymers. For the sake of illustration, we considered the simplest non-linear kinetic theory of a dilute polymer solution, known as the FENE dumbbell model [2]. A new closure approximation for the FENE theory, referred to as the FENE-L model, was introduced in [1] for one-dimensional elongational flows. Simulations revealed that the FENE-L model is a considerably more

*Dedicated to professor David V. Boger on the occasion of his 60th birthday.

accurate approximation of the FENE theory than the classical FENE-P constitutive equation derived using the Peterlin [3] closure scheme. In particular, it is capable of reproducing the hysteretic behaviour of the FENE theory in stress versus birefringence curves during start-up of flow and subsequent relaxation (see also [4]).

The goal of the present paper is to extend the one-dimensional FENE-L theory proposed in [1] to general, three-dimensional flow kinematics. The paper is organized as follows. In Section 2, we summarize the kinetic theory of FENE dumbbells. Following the generic approach adopted in the companion paper [1], suitable state variables are selected in Section 3, each of which obeying an evolution equation derived from the diffusion equation. In Section 4, we introduce a particular canonical subspace wherein length and orientation of the dumbbells are decoupled. It is shown that use of a decoupled canonical subspace yields a scalar closure problem, to which the one-dimensional theory of Lielens *et al.* readily applies. The classical FENE-P closure model is recovered in Section 5 using the configuration tensor as single state variable. In Section 6, we derive the three-dimensional version of the FENE-L model, and propose a simplified version of that theory referred to as FENE-LS. Finally, we compare in Section 7 the response of the FENE-P, FENE-L, and FENE-LS closure models to that of the actual FENE kinetic theory in steady-state and transient rheometrical flows (shear and elongation).

2 Kinetic theory of FENE dumbbells

In the present paper, we address the closure problem for the kinetic theory of Warner Finitely Extensible Non-linear Elastic (FENE) dumbbells [2]. This is the most elementary non-linear kinetic model of a dilute polymer solution wherein the polymer is described by two identical Brownian beads connected by a spring. The beads experience Brownian forces and the Stokes drag exerted by the solvent, while the entropic spring models intramolecular interactions. The configuration of the polymer is given by the length and orientation of the vector $\boldsymbol{Q}$ that connects the two beads. For FENE dumbbells, the spring force $\boldsymbol{F}^c$ is defined as

$$\boldsymbol{F}^c(\boldsymbol{Q}) = \frac{H}{1 - \boldsymbol{Q}^2/Q_0^2}\,\boldsymbol{Q}, \tag{1}$$

where H is a spring constant and Q_0 is the maximum spring length. The polymer contribution $\boldsymbol{\tau}_p$ to the stress tensor is computed through Kramers' expression [2]:

$$\boldsymbol{\tau}_p = n\ \langle \boldsymbol{Q}\boldsymbol{F}^c(\boldsymbol{Q})\rangle - nkT\boldsymbol{I}, \tag{2}$$

where n is the dumbbell number density, k is the Boltzmann constant, T is the absolute temperature, and the angular brackets denote the configuration space average

$$\langle\ \cdot\ \rangle = \int \cdot\ \psi(\boldsymbol{Q})\ d\boldsymbol{Q}. \tag{3}$$

Here, $\psi(\boldsymbol{Q})$ is the distribution function, i.e. $\psi(\boldsymbol{Q})d\boldsymbol{Q}$ is the probability of finding the $\boldsymbol{Q}$ vector between $\boldsymbol{Q}$ and $\boldsymbol{Q}+d\boldsymbol{Q}$. The distribution function belongs to the space Ψ of functions that are always positive, even in $\boldsymbol{Q}$, and of unit integral over the configuration space $\{\boldsymbol{Q} \mid \boldsymbol{Q}\cdot\boldsymbol{Q} \leq Q_0^2\}$. In order to compute the extra-stress tensor $\boldsymbol{\tau}$, one adds to $\boldsymbol{\tau}_p$ the contribution $\boldsymbol{\tau}_s$ of the Newtonian solvent:

$$\boldsymbol{\tau} = \boldsymbol{\tau}_s + \boldsymbol{\tau}_p, \qquad\qquad \boldsymbol{\tau}_s = 2\eta_s \boldsymbol{D}, \tag{4}$$

where $\boldsymbol{D}$ is the rate of deformation tensor $\frac{1}{2}\left(\nabla\boldsymbol{v} + \nabla\boldsymbol{v}^T\right)$ and η_s is the constant shear viscosity of the solvent.

The FENE theory involves a relaxation time $\lambda = \xi/(4H)$ and a dimensionless finite extensibility parameter $b = HQ_0^2/(kT)$, where ξ is the beads friction coefficient. In the remainder of the paper, we shall write all equations in dimensionless form. The connector vector $\boldsymbol{Q}$, the time t, the velocity gradient $\boldsymbol{\kappa}$ and the polymer stress $\boldsymbol{\tau}_p$ are made dimensionless with $(kT/H)^{1/2}$, λ, λ^{-1}, and nkT, respectively. We can thus view the magnitude of the dimensionless velocity gradient $\boldsymbol{\kappa}$ as a Weissenberg number We. In dimensionless form, the diffusion equation that governs the evolution of ψ along the flow trajectories reads [2]

$$\frac{D\psi}{Dt} = \frac{1}{2}\frac{\partial}{\partial\boldsymbol{Q}}\cdot\frac{\partial}{\partial\boldsymbol{Q}}\psi - \frac{\partial}{\partial\boldsymbol{Q}}\cdot\left(\left[\boldsymbol{\kappa}\cdot\boldsymbol{Q} - \frac{1}{2}\boldsymbol{F}^c(\boldsymbol{Q})\right]\psi\right), \tag{5}$$

while the FENE spring force (1) and Kramers' expression (2) become

$$\boldsymbol{F}^c(\boldsymbol{Q}) = \frac{\boldsymbol{Q}}{1-\boldsymbol{Q}^2/b}\,, \tag{6}$$

$$\boldsymbol{\tau}_p = \langle\boldsymbol{Q}\boldsymbol{F}^c(\boldsymbol{Q})\rangle - \boldsymbol{I}\,. \tag{7}$$

As discussed in [2], it is only in the limit of linear Hookean springs ($b\to\infty$) that the FENE kinetic theory yields an equivalent constitutive equation for $\boldsymbol{\tau}_p$; when written in terms of the extra-stress $\boldsymbol{\tau} = \boldsymbol{\tau}_s + \boldsymbol{\tau}_p$, this equation is the classical Oldroyd-B model. For finite values of the extensibility parameter b, constitutive equations that approximate the FENE kinetic theory can be derived by resorting to suitable closure approximations. In the present context, a classical closure approximation due to Peterlin consists in pre-averaging the non-linear spring law,

$$\boldsymbol{F}^c(\boldsymbol{Q}) = \frac{\boldsymbol{Q}}{1-\langle\boldsymbol{Q}^2\rangle/b}\,, \tag{8}$$

yielding the FENE-P constitutive equation. It has been shown recently [5, 3, 1, 4] that the impact of the Peterlin approximation is significant, that is, the FENE-P model can be a poor approximation of the FENE kinetic theory, especially in transient flows. In the present paper, we extend the one-dimensional (1d) theory proposed by Lielens et al. [1] for deriving improved closure models.

3 State variables and evolution equations

Following [1], the fluid is described by a finite set X of n state variables X_i ,

$$X = \{X_1, X_2, ..., X_n\} = \{A, B, C, ...\} ,$$

where X_i is the configuration space average of a scalar or tensorial function f_i of the connector vector $\boldsymbol{Q}$:

$$X_i = \langle f_i(\boldsymbol{Q}) \rangle . \tag{9}$$

The state variable X_i is solution to the following evolution equation [2], derived from the diffusion equation (5):

$$\frac{DX_i}{Dt} = \underbrace{\frac{1}{2}\left\langle \frac{\partial}{\partial \boldsymbol{Q}} \cdot \frac{\partial}{\partial \boldsymbol{Q}} f_i(\boldsymbol{Q}) \right\rangle}_{X_i^B} + \boldsymbol{\kappa} : \underbrace{\left\langle \boldsymbol{Q} \frac{\partial}{\partial \boldsymbol{Q}} f_i(\boldsymbol{Q}) \right\rangle}_{X_i^D} - \underbrace{\frac{1}{2}\left\langle \boldsymbol{F}^c(\boldsymbol{Q}) \cdot \frac{\partial}{\partial \boldsymbol{Q}} f_i(\boldsymbol{Q}) \right\rangle}_{X_i^C}. \tag{10}$$

The right-hand side of Eq. (10) involves three new state variables X_i^B, X_i^D and X_i^C, related respectively to Brownian motion, hydrodynamic drag and connector force. The closure problem amounts to establish a relationship between $\left\{X_i^B, X_i^D, X_i^C\right\}$ and the original set X of state variables.

According to the 1d theory [1], we select as first state variable X_1 the second moment of the distribution function,

$$X_1 = \boldsymbol{A} = \langle \boldsymbol{Q}\boldsymbol{Q} \rangle . \tag{11}$$

The evolution equation (10) for X_1 then reads

$$\frac{D\boldsymbol{A}}{Dt} = \boldsymbol{I} + \boldsymbol{\kappa} \cdot \boldsymbol{A} + \boldsymbol{A} \cdot \boldsymbol{\kappa}^T - \underbrace{\langle \boldsymbol{Q}\boldsymbol{F}^c(\boldsymbol{Q}) \rangle}_{\boldsymbol{A}^C}. \tag{12}$$

Clearly, only the connector state variable $X_1^C \sim \boldsymbol{A}^C$ introduces a closure problem for a non-linear force law $\boldsymbol{F}^c(\boldsymbol{Q})$. Also in accordance with the 1d theory, we choose as second state variable X_2 a scalar measure of the radial dispersion of the dumbbells:

$$X_2 = B = \left\langle (\boldsymbol{Q} \cdot \boldsymbol{Q})^2 \right\rangle . \tag{13}$$

The evolution equation (10) for B reads

$$\frac{DB}{Dt} = 10\, tr(\boldsymbol{A}) + 4\boldsymbol{\kappa} : \underbrace{\langle \boldsymbol{Q}\boldsymbol{Q}\,(\boldsymbol{Q}\cdot\boldsymbol{Q})\rangle}_{B^D} - 2\underbrace{\left\langle \frac{(\boldsymbol{Q}\cdot\boldsymbol{Q})^2}{1-\boldsymbol{Q}^2/b}\right\rangle}_{B^C}. \tag{14}$$

Here, a closure is needed for the drag and connector state variables, namely $X_2^D \sim B^D$ and $X_2^C \sim B^C$. Finally, Kramers' expression (7) becomes

$$\boldsymbol{\tau}_p = \boldsymbol{A}^C - \boldsymbol{I}. \tag{15}$$

The present closure problem is indeed much more complex than its one-dimensional counterpart in view of the tensorial nature of the state variables $\boldsymbol{A}$ and $\boldsymbol{A}^C$. We shall address this difficulty by selecting an appropriate *decoupled* canonical subspace Ψ^c for the distribution function.

4 Decoupled canonical subspace

Following [1], we restrict the space Ψ of admissible distribution functions ψ to a so-called canonical subset Ψ^c of finite dimension m. This subspace is made of all instances of a canonical distribution function ψ^c which has m independent parameters. The present closure problem is made considerably simpler by selecting a canonical distribution that is decoupled in length and orientation:

$$\psi^c(\boldsymbol{Q}) = \psi^Q(Q)\,\psi^{\boldsymbol{u}}(\boldsymbol{u}), \tag{16}$$

where $Q = \|\boldsymbol{Q}\| = \sqrt{\boldsymbol{Q}\cdot\boldsymbol{Q}}$ and $\boldsymbol{u} = \boldsymbol{Q}/Q$ are the dumbbell's length and unit orientation vector, respectively. We shall use a normalized orientation distribution function

$$\psi^{\boldsymbol{u}}(\boldsymbol{u}) \geqslant 0\ ,\ \oint \psi^{\boldsymbol{u}}(\boldsymbol{u})\, d\boldsymbol{u} = 1, \tag{17}$$

where $\oint \cdot\, d\boldsymbol{u}$ denotes the integral over the unit sphere. Thus, ψ^Q must obey

$$\psi^Q(Q) \geqslant 0\ ,\ \int_0^{\sqrt{b}} Q^2 \psi^Q(Q)\, dQ = 1, \tag{18}$$

so that $\psi^c(\boldsymbol{Q})$ belongs to the space Ψ of admissible distribution functions.

The major consequence of selecting a decoupled canonical subspace is that the approximations of $\boldsymbol{A}$ and $\boldsymbol{A}^C$, obtained by means of ψ^c instead of ψ, are *proportional*. Indeed, we have

$$\begin{aligned}\boldsymbol{A} \approx \langle \boldsymbol{Q}\boldsymbol{Q}\rangle_c &= \int \boldsymbol{Q}\boldsymbol{Q}\,\psi^Q(Q)\,\psi^{\boldsymbol{u}}(\boldsymbol{u})\, d\boldsymbol{Q} \\ &= \int_0^{\sqrt{b}} Q^4\,\psi^Q(Q)\, dQ \oint \boldsymbol{u}\,\boldsymbol{u}\,\psi^{\boldsymbol{u}}(\boldsymbol{u})\, d\boldsymbol{u}\,,\end{aligned} \tag{19}$$

On the other hand, the connector state variable $\boldsymbol{A}^C$ is approximated as

$$\begin{aligned}\boldsymbol{A}^C \approx \langle \boldsymbol{Q}\boldsymbol{F}^c(\boldsymbol{Q})\rangle_c &= \int \boldsymbol{Q}\ \left(\|\boldsymbol{F}^{\boldsymbol{c}}(\boldsymbol{Q})\|\,\boldsymbol{u}\right)\ \psi^Q(Q)\,\psi^{\boldsymbol{u}}(\boldsymbol{u})\,d\boldsymbol{Q} \\ &= \int_0^{\sqrt{b}} Q^3 F^c(Q)\ \psi^Q(Q)\,dQ \oint \boldsymbol{u}\,\boldsymbol{u}\,\psi^{\boldsymbol{u}}(\boldsymbol{u})\,d\boldsymbol{u}\ ,\end{aligned} \tag{20}$$

where $F^c(Q) = Q/\left(1 - Q^2/b\right)$ is the norm of the connector force. In deriving (20), account has been made of the colinearity of $\boldsymbol{F^c}$ and $\boldsymbol{Q}$. Comparing Eqs. (19) and (20), we finally obtain the following proportionality rule between $\boldsymbol{A}$ and $\boldsymbol{A}^C$ in the decoupled canonical subspace:

$$\boldsymbol{A}^C = \frac{\int_0^{\sqrt{b}} Q^3 F^c(Q)\ \psi^Q(Q)\,dQ}{\int_0^{\sqrt{b}} Q^4\,\psi^Q(Q)\,dQ}\ \boldsymbol{A} = \vartheta\boldsymbol{A}, \tag{21}$$

where ϑ is a scalar proportionality coefficient (always larger than one, due to the particular form of $F^c(Q)$) depending on the radial distribution ψ^Q.

Use of the decoupled canonical distribution (16) is of course expected to yield approximate results only. In particular, closure models derived from (16) necessarily have a vanishing second normal stress difference N_2 in transient simple shear flows. Indeed, in view of (12), (15) and (21), we have

$$\frac{D\boldsymbol{A}}{Dt} = \boldsymbol{I} + \boldsymbol{\kappa}\cdot\boldsymbol{A} + \boldsymbol{A}\cdot\boldsymbol{\kappa}^T - \vartheta\boldsymbol{A}\ ,\ \boldsymbol{\tau}_p = \vartheta\boldsymbol{A} - \boldsymbol{I}. \tag{22}$$

For the simple shear flow $[v_x, v_y, v_z] = [\dot{\gamma}(t)\,y, 0, 0]$, Eq. (22) yields

$$\frac{D}{Dt}\frac{N_2}{\vartheta} = \frac{D}{Dt}\frac{\tau_{p,yy} - \tau_{p,zz}}{\vartheta} = \frac{D}{Dt}\left(A_{yy} - A_{zz}\right) = -\vartheta\left[A_{yy} - A_{zz}\right] = -N_2 \tag{23}$$

So, $N_2(t) \equiv 0$ in all simple shear flows starting from isotropic equilibrium conditions (The FENE kinetic theory generally predicts $N_2(t) \neq 0$ in transient shear flows; the steady-state value of N_2 also vanishes, however [5]).

In order to proceed, we define the normalized radial distribution

$$\rho^c(Q) = Q^2\psi^Q(Q)\,,\ \text{with}\ \int_0^{\sqrt{b}} \rho^c(Q)\ dQ = 1. \tag{24}$$

In view of Eqs. (19) and (20), the following relations are obtained:

$$\begin{aligned} tr(\boldsymbol{A}) &\approx \int_0^{\sqrt{b}} Q^2\,\rho^c(Q)\,dQ, \\ tr(\boldsymbol{A}^C) &\approx \int_0^{\sqrt{b}} \frac{Q^2}{1 - Q^2/b}\,\rho^c(Q)\,dQ, \end{aligned} \tag{25}$$

which are analogous to Eq. (20a) of the 1d theory [1], with the radial distribution $\rho^c(Q)$ playing the role of the 1d distribution function $\psi^c(Q)$.

Let us now show that the decoupling approximation (16) in fact solves the closure problem for the drag state variable B^D in Eq. (14). Indeed, we have in the canonical subspace,

$$B \approx \left\langle (\boldsymbol{Q}\cdot\boldsymbol{Q})^2 \right\rangle_c = \int_0^{\sqrt{b}} Q^4\, \rho^c(Q)\, dQ. \tag{26}$$

Thus, in view of Eqs. (19) and (25),

$$\begin{aligned} B^D \approx \langle (\boldsymbol{Q}\cdot\boldsymbol{Q})\boldsymbol{Q}\boldsymbol{Q} \rangle_c &= \int_0^{\sqrt{b}} Q^4\, \rho^c(Q)\, dQ \oint \boldsymbol{u}\,\boldsymbol{u}\,\psi^{\boldsymbol{u}}(\boldsymbol{u})\, d\boldsymbol{u} \\ &= \frac{B}{tr(\boldsymbol{A})}\boldsymbol{A}. \end{aligned} \tag{27}$$

We then obtain the following evolution equation for $\boldsymbol{A}$ and B

$$\begin{aligned} \frac{D\boldsymbol{A}}{Dt} &= \boldsymbol{I} + \boldsymbol{\kappa}\cdot\boldsymbol{A} + \boldsymbol{A}\cdot\boldsymbol{\kappa}^T - \frac{\boldsymbol{A}}{tr(\boldsymbol{A})} \underbrace{\int_0^{\sqrt{b}} \frac{Q^2}{1-Q^2/b}\, \rho^c(Q)\, dQ}_{A^C}, \\ \frac{DB}{Dt} &= 10\, tr(\boldsymbol{A}) + 4\frac{B}{tr(\boldsymbol{A})}\boldsymbol{\kappa} : \boldsymbol{A} - 2 \underbrace{\int_0^{\sqrt{b}} \frac{Q^4}{1-Q^2/b}\, \rho^c(Q)\, dQ}_{B^C}, \end{aligned} \tag{28}$$

while Kramers' expression (15) becomes

$$\boldsymbol{\tau}_p = \frac{\boldsymbol{A}}{tr(\boldsymbol{A})} \underbrace{\int_0^{\sqrt{b}} \frac{Q^2}{1-Q^2/b}\, \rho^c(Q)\, dQ}_{A^C} - \boldsymbol{I}\,. \tag{29}$$

Clearly, only the *scalar* connector state variables, A^C and B^C, need closure.

In summary, use of a decoupled canonical subspace reduces the present closure problem to a purely scalar problem. Furthermore, only the radial distribution $\rho(Q)$ needs restriction to a canonical subspace; the orientation distribution $\psi^{\boldsymbol{u}}$ is left unspecified.

5 First-order closure

For the sake of illustration, we derive the classical FENE-P model [2] by describing the fluid with a single state variable $\boldsymbol{A}$. The following one-parameter canonical radial distribution is defined:

$$\rho_\alpha^c(Q) = \delta_\alpha(Q), \tag{30}$$

where $\delta_\alpha(Q)$ is the Dirac distribution located at $Q = \alpha$. This particular choice of decoupled canonical subspace assumes that all dumbbells have the same length, although they can have an arbitrary orientation. In view of Eqs. (21) and (25), we readily obtain the classical Peterlin closure approximation:

$$\boldsymbol{A}^C \approx \frac{1}{1 - tr\left(\boldsymbol{A}\right)/b}\boldsymbol{A}\,, \tag{31}$$

and use of Eqs. (10) and (29) yields the FENE-P model:

$$\begin{aligned} \frac{D\boldsymbol{A}}{Dt} &= \boldsymbol{I} + \boldsymbol{\kappa}\cdot\boldsymbol{A} + \boldsymbol{A}\cdot\boldsymbol{\kappa}^T - \frac{1}{1 - tr(\boldsymbol{A})/b}\boldsymbol{A}, \\ \boldsymbol{\tau}_p &= \frac{1}{1 - tr(\boldsymbol{A})/b}\boldsymbol{A} - \boldsymbol{I}. \end{aligned} \tag{32}$$

We wish to note that Tanner [6] derived the FENE-P model by assuming that the dumbbells share the same length *and* the same orientation. Although his final result is correct, this assumption is inconsistent. For example, it is in contradiction with the fact that $\boldsymbol{A}$ is isotropic at equilibrium.

6 Second-order closure

6.1 General formulation

We now wish to develop a second-order closure with $\boldsymbol{A} = \langle \boldsymbol{Q}\boldsymbol{Q} \rangle$ and $B = \left\langle (\boldsymbol{Q}\cdot\boldsymbol{Q})^2 \right\rangle$ as state variables. In view of the use of the decoupled canonical subspace (Section 4), we can follow as such the approach of the 1d theory [1]. A two-parameter canonical radial distribution $\rho^c_{\alpha,\beta}\left(Q\right)$ is selected, which, in view of Eqs. (25), (26) and (28), gives the following approximations of the state variables:

$$\begin{aligned} tr(\boldsymbol{A}) &\approx \int_0^{\sqrt{b}} Q^2\, \rho^c_{\alpha,\beta}\left(Q\right)\, dQ, \\ B &\approx \int_0^{\sqrt{b}} Q^4\, \rho^c_{\alpha,\beta}\left(Q\right)\, dQ, \\ A^C &\approx \int_0^{\sqrt{b}} \frac{Q^2}{1 - Q^2/b}\, \rho^c_{\alpha,\beta}\left(Q\right)\, dQ, \\ B^C &\approx \int_0^{\sqrt{b}} \frac{Q^4}{1 - Q^2/b}\, \rho^c_{\alpha,\beta}\left(Q\right)\, dQ. \end{aligned} \tag{33}$$

As in [1], the first two relations are inverted to yield the parameters α and β as a function of $tr(\boldsymbol{A})$ and B. The last two relations of Eq. (33) then yield the closure expressions $A^C\left(tr(\boldsymbol{A}),B\right)$ and $B^C\left(tr(\boldsymbol{A}),B\right)$.

The final form of the second-order closure model (28) and (29) obtained with the decoupled canonical subspace (16) reads

$$\begin{aligned}
\frac{D\boldsymbol{A}}{Dt} &= \boldsymbol{I}+\boldsymbol{\kappa}\cdot\boldsymbol{A}+\boldsymbol{A}\cdot\boldsymbol{\kappa}^T-\frac{A^C\left(tr(\boldsymbol{A}),B\right)}{tr(\boldsymbol{A})}\boldsymbol{A},\\
\frac{DB}{Dt} &= 10\,tr(\boldsymbol{A})+4\frac{B}{tr(\boldsymbol{A})}\boldsymbol{\kappa}:\boldsymbol{A}-2B^C\left(tr(\boldsymbol{A}),B\right),\\
\boldsymbol{\tau}_p &= \frac{A^C\left(tr(\boldsymbol{A}),B\right)}{tr(\boldsymbol{A})}\boldsymbol{A}-\boldsymbol{I}\,.
\end{aligned} \tag{34}$$

The actual form of $A^C\left(tr(\boldsymbol{A}),B\right)$ and $B^C\left(tr(\boldsymbol{A}),B\right)$ is obtained by specifying the canonical radial distribution function $\rho^c_{\alpha,\beta}$. Two examples are discussed next, yielding respectively the FENE-L and FENE-LS models.

6.2 FENE-L closure

In accordance with the 1d theory [1], the canonical, FENE-L radial distribution is defined as follows

$$\rho^c_{\alpha,\beta}(Q)=\frac{(1-\beta)}{\alpha}\left[1-H_\alpha(Q)\right]+\beta\,\delta_\alpha(Q), \tag{35}$$

where $(\alpha,\beta)\in[0,\sqrt{b}]\times[0,1]$ and $H_\alpha(Q)$ denotes the Heaviside unit step function located at $Q=\alpha$ (Fig. 1).

Insert Figure 1

With this particular choice, the relations (33) become

$$\begin{aligned}
tr\left(\boldsymbol{A}\right) &\approx \beta\alpha^2+\frac{(1-\beta)\alpha^2}{3},\\
B &\approx \beta\alpha^4+\frac{(1-\beta)\alpha^4}{5},\\
A^C &\approx \frac{\beta\alpha^2}{1-\alpha^2/b}+(1-\beta)b\left[\frac{\sqrt{b}}{\alpha}\ln\left(\frac{\sqrt{b}+\alpha}{\sqrt{b}-\alpha}\right)-1\right],\\
B^C &\approx \frac{\beta\alpha^4}{1-\alpha^2/b}+(1-\beta)b^2\left[\frac{\sqrt{b}}{\alpha}\ln\left(\frac{\sqrt{b}+\alpha}{\sqrt{b}-\alpha}\right)-1-\frac{\alpha}{3\sqrt{b}}\right].
\end{aligned} \tag{36}$$

Following [1], Eqs. (36a) and (36b) give α and β as a function of $A = tr(\boldsymbol{A})$ and B:

$$\begin{aligned} \alpha^2 &= \frac{5B}{3A + \sqrt{9A^2 - 5B}}, \\ \beta &= \frac{(9A^2 - 5B) + \sqrt{(9A^2 - 5B)9A^2}}{10B}. \end{aligned} \tag{37}$$

The FENE-L closure expressions $A^C\left(tr(\boldsymbol{A}), B\right)$ and $B^C\left(tr(\boldsymbol{A}), B\right)$ are then obtained by substituting Eq. (37) in Eqs. (36c) and (36d). As explained in [1], it is necessary to add the following constraint to the FENE-L model

$$B < \frac{9}{5}A^2\,, \tag{38}$$

in order to prevent the pair $(tr(\boldsymbol{A}), B)$ from leaving its space of admissible values. The FENE-L closure expressions $A^C\left(tr(\boldsymbol{A}), B\right)$ and $B^C\left(tr(\boldsymbol{A}), B\right)$ are not detailed here, being rather lengthy. A somewhat simpler closure model, referred to as FENE-LS, is proposed in the next section.

6.3 FENE-LS closure

Our goal in deriving the FENE-LS model is to simplify the closure expressions $A^C\left(tr(\boldsymbol{A}), B\right)$ and $B^C\left(tr(\boldsymbol{A}), B\right)$ of the FENE-L theory while keeping most of the underlying physics. To this end, the FENE-LS canonical distribution is defined as follows

$$\rho^c_{\alpha,\beta}(Q) = \ (1-\beta)\ \delta_{\alpha/R}(Q)\ + \beta\ \delta_\alpha(Q), \tag{39}$$

where $(\alpha, \beta) \in [0, \sqrt{b}] \times [0, 1]$ and R is a constant that will be specified later (Fig. 2).

Insert Figure 2

Here, the tail of the FENE-L distribution has been approximated by a Dirac distribution located at α/R; the limit $R \to \infty$ yields the FENE-P^2 model studied in the 1d theory [1]. For the FENE-LS model, the relations (33) become

$$\begin{aligned} tr\left(\boldsymbol{A}\right) &\approx \alpha^2 \left(\beta + \frac{(1-\beta)}{R^2}\right), \\ B &\approx \alpha^4 \left(\beta + \frac{(1-\beta)}{R^4}\right), \\ A^C &\approx \alpha^2 \left(\beta \frac{1}{1-\alpha^2/b} + \frac{(1-\beta)}{R^2}\frac{1}{1-\alpha^2/(R^2 b)}\right), \\ B^C &\approx \alpha^4 \left(\beta \frac{1}{1-\alpha^2/b} + \frac{(1-\beta)}{R^4}\frac{1}{1-\alpha^2/(R^2 b)}\right). \end{aligned} \tag{40}$$

The first two relations yield α and β as a function of $A = tr(\boldsymbol{A})$ and $d = \dfrac{B}{A^2}$:

$$\begin{aligned} \alpha^2 &= A \frac{R^2 d}{\dfrac{R^2+1}{2} + \dfrac{R^2+1}{2}\sqrt{1 - \dfrac{4R^2 d}{(R^2+1)^2}}}, \\ \beta &= \frac{R^2 \dfrac{A}{\alpha^2} - 1}{R^2 - 1}. \end{aligned} \tag{41}$$

If we choose $R^2 = 5$, we obtain

$$\alpha^2 = \frac{5B}{3A + \sqrt{9A^2 - 5B}},$$

which is exactly the same expression as for the FENE-L model. This gives us an indication as to the choice of R for obtaining a good approximation of the FENE-L closure, and hence of the FENE theory. The FENE-LS closure approximation is then obtained by substituting (41) in (36c) and (36d).

Here again, it is necessary to add the following constraint to the FENE-LS constitutive equation:

$$B < \frac{\left(\dfrac{R^2+1}{2}\right)^2}{R^2} A^2 . \tag{42}$$

In order to simplify the closure even more and get rid of the annoying constraint, it is attractive to approximate the square root present in the expression (41a) for α^2 as follows

$$\sqrt{1 - \frac{R^2 d}{\left(\dfrac{R^2+1}{2}\right)^2}} \approx 1 - \gamma \frac{R^2 d}{\left(\dfrac{R^2+1}{2}\right)^2},$$

where γ is a constant around 0.5 which will be determined later. With this approximation, Eq. (41a) becomes

$$\alpha^2 = A \frac{R^2 d}{R^2 + 1 - 2\gamma \dfrac{R^2 d}{R^2+1}} .$$

This expression allows us to naturally specify the coefficient γ. When $d = \dfrac{B}{A^2} = 1$, the radial distribution must be a single Dirac distribution [1], i.e. with $\beta = 1$ and

$\alpha^2 = A$. To achieve that, we must impose $\gamma = \dfrac{R^2+1}{2R^2}$, which is indeed close to 0.5 if R^2 is sufficiently large. The expressions (41) then become

$$\begin{aligned} \alpha^2 &= A\frac{R^2}{\dfrac{R^2+1}{d}-1} = A\frac{1-K}{f-K}, \\ \beta &= \frac{\dfrac{R^2+1}{d}-2}{R^2-1} = \frac{f-2K}{1-2K}, \end{aligned} \tag{43}$$

with $K = (R^2+1)^{-1}$ and $f = d^{-1} = A^2/B$.

Inserting these results in (40a-b) gives the FENE-LS closure. Before that, one further simplification that we made is $\dfrac{1}{1-\alpha^2/(R^2 b)} \approx 1$, valid if R^2 is sufficiently large. This gives

$$\begin{aligned} A^C &\approx \alpha^2\left(\beta\frac{1}{1-\alpha^2/b} + \frac{(1-\beta)}{R^2}\right), \\ B^C &\approx \alpha^4\left(\beta\frac{1}{1-\alpha^2/b} + \frac{(1-\beta)}{R^4}\right), \end{aligned}$$

and finally, with the help of (43), we obtain the FENE-LS closure approximation in explicit form

$$\begin{aligned} A^C &= \left(A\frac{1-K}{f-K}\right)\left[\frac{f-2K}{1-2K}\left(1-\frac{A}{b}\frac{1-K}{f-K}\right)^{-1} + \frac{(1-f)}{R^2(1-2K)}\right], \\ B^C &= \left(A\frac{1-K}{f-K}\right)^2\left[\frac{f-2K}{1-2K}\left(1-\frac{A}{b}\frac{1-K}{f-K}\right)^{-1} + \frac{(1-f)}{R^4(1-2K)}\right]. \end{aligned} \tag{44}$$

In the sequel, we set $R^2 = 5$ in the FENE–LS equation.

7 Simulation results for rheometrical flows

We compare in this section the predictions of the FENE–P, FENE–L and FENE–LS closure models to those of the FENE kinetic theory in several steady-state and time-dependent rheometrical flows with specified kinematics. In all cases, we set $b = 50$ and the initial conditions for the transient simulations correspond to equilibrium. The response of the FENE model is computed by means of the predictor-corrector stochastic simulation technique proposed by Öttinger [7], and detailed in Section 3 of [3];

we use 10^4 realizations for each stochastic simulation, which provides accurate results for the relevant ensembles averages $\langle \boldsymbol{QQ} \rangle$, $\left\langle (\boldsymbol{Q} \cdot \boldsymbol{Q})^2 \right\rangle$ and $\langle \boldsymbol{QF}^c(\boldsymbol{Q}) \rangle$. We solve the FENE-P and FENE-LS constitutive equations (32) and (28, 44) by means of a fifth-order Runge-Kutta technique with adaptive time stepping. For solving the constrained FENE-L constitutive equation (28, 36, 38), the penalty method developed for the 1d theory [1] could be used. We have found, however, that, in contrast with the 1d case, the FENE-L constraint never becomes active in three-dimensional flow kinematics. The FENE-L constitutive equation has thus been solved by means of the same Runge-Kutta technique as for the FENE-P and FENE-LS equations.

7.1 Steady simple shear

We consider first a steady simple shear flow with kinematics $[v_x, v_y, v_z] = [\dot{\gamma} y, 0, 0]$, where $\dot{\gamma} = \kappa_{xy}$ is the specified, constant shear rate. The relevant material functions are the viscosity η, and the first and second normal stress coefficients ψ_1, ψ_2. These are given in dimensionless form by

$$\begin{aligned} \frac{\eta(\dot{\gamma}) - \eta_s}{nkT\lambda} &= \frac{1}{\lambda\dot{\gamma}} \frac{\tau_{p,xy}}{nkT}, \\ \frac{\psi_1(\dot{\gamma})}{nkT\lambda^2} &= \frac{1}{(\lambda\dot{\gamma})^2} \frac{\tau_{p,xx} - \tau_{p,yy}}{nkT}, \\ \frac{\psi_2(\dot{\gamma})}{nkT\lambda^2} &= \frac{1}{(\lambda\dot{\gamma})^2} \frac{\tau_{p,yy} - \tau_{p,zz}}{nkT}. \end{aligned} \tag{45}$$

As shown in Fig. 3, the shear viscosity computed with the FENE-L and FENE-LS constitutive equations is in excellent agreement with the result of the FENE kinetic theory. The FENE-P fluid shows a similar behaviour, although it is slightly less accurate an approximation at intermediate values of the shear rate [5].

Insert Figure 3

Results for the first normal stress coefficient ψ_1 are shown in Fig. 4. Here again, the FENE-L and FENE-LS models are slightly closer to the response of the FENE theory than the FENE-P fluid for low to moderate shear rates ($\lambda\dot{\gamma} < 10$). At large shear rates, all closure models give identical results which overpredict the first normal stress coefficient of the FENE theory. This is due, we believe, to the decoupling approximation (16) which is shared by the three closure approximations.

Insert Figure 4

As noted in Section 4, all four models predict a vanishing second normal stress coefficient ψ_2 in steady-state shear flow (see also [5]).

7.2 Steady uniaxial elongation

The velocity field for steady uniaxial elongation is given by $[v_x, v_y, v_z] = \left[\dot{\varepsilon}x, -\frac{1}{2}\dot{\varepsilon}y, -\frac{1}{2}\dot{\varepsilon}z\right]$, where $\dot{\varepsilon} = \kappa_{xx}$ is the specified, constant elongation rate. The relevant material function is the elongational viscosity $\bar{\eta}$, which is given in dimensionless form by

$$\frac{\bar{\eta}\left(\dot{\varepsilon}\right) - 3\eta_s}{nkT\lambda} \quad = \quad \frac{1}{\lambda\dot{\varepsilon}} \frac{\tau_{p,xx} - \tau_{p,yy}}{nkT}. \tag{46}$$

Insert Figure 5

Inspection of Fig. 5 reveals that the four models show very similar behaviour. The FENE-L and FENE-LS closures better approximate the FENE theory for extension rates smaller than one. At intermediate extension rates ($1 < \lambda\dot{\varepsilon} < 5$), none of the three closures is clearly superior (this was already noticed and discussed in the context of the 1d theory; See Section 5.3 in [1].). For $\lambda\dot{\varepsilon} > 5$, the three closures give excellent results.

It is in fact in *time-dependent* flows that important quantitative and qualitative differences appear between the FENE-P closure and the more elaborate FENE-L and FENE-LS models, as discussed next.

7.3 Start-up of simple shear followed by relaxation

We now consider the inception from equilibrium conditions of simple shear flow with a constant shear rate $\dot{\gamma}$, followed by relaxation after $t/\lambda = 4$. Figures 6 to 8 show the temporal evolution of the first normal stress difference $\left(\tau_{p,xx} - \tau_{p,yy}\right)/nkT\lambda$ and shear stress $\tau_{p,xy}/nkT\lambda$ for $\lambda\dot{\gamma} = 2$, 5 and 10.

Insert Figure 6

Insert Figure 7

Insert Figure 8

Time-dependent shear is clearly a challenge for all the available closures. The FENE-L and FENE-LS closures are far more accurate than the FENE-P model, but agreement with the FENE results is only qualitative. Here again, the FENE-L and FENE-LS results are almost identical.

7.4 Start-up of uniaxial elongation followed by relaxation

Here we study the inception from equilibrium conditions of uniaxial elongation with a constant elongation rate $\dot{\varepsilon}$, followed by relaxation after $t/\lambda = 1.5$. Figure 9 shows the temporal evolution of the transient elongational viscosity

$$\frac{\bar{\eta}^{+} - 3\eta_s}{nkT\lambda} = \frac{1}{\lambda\dot{\varepsilon}} \frac{\tau_{p,xx}(t) - \tau_{p,yy}(t)}{nkT},$$

as well as that of the mean square molecular extension $tr\langle H\boldsymbol{QQ}/kT\rangle$, for $\lambda\dot{\varepsilon} = 6$.

Insert Figure 9

While all closures give identical results in the relaxation phase, the FENE-L and FENE-LS closures are remarkably more accurate during stress growth.

Insert Figure 10

As discussed in details in [1, 4], a distinct property of the FENE kinetic theory is the hysteretic behaviour of stress versus molecular extension predicted in this experiment. In Fig. 10, we plot the results of Fig. 9 in the form of curves of elongational viscosity versus average molecular extension parameterized by time. The FENE-P model does not show hysteretic behaviour at all; the FENE-L and FENE-LS closures predict hysteresis curves in qualitative agreement with the FENE kinetic theory.

The behaviour of the FENE-L/LS closures in 3d transient elongation is indeed very similar to that predicted in the context of the one-dimensional theory [1]. It is for this class of flows, which motivated the design of the canonical radial distributions (35) and (39), that the new closures are at their best.

7.5 Start-up of biaxial elongation followed by relaxation

Finally, we consider the inception from equilibrium conditions of biaxial elongation characterized by the velocity gradient $\boldsymbol{\kappa} = diag(\dot{\varepsilon}, \dot{\varepsilon}, -2\dot{\varepsilon})$, where $\dot{\varepsilon}$ is the constant elongation rate, followed by relaxation after $t/\lambda = 1.5$. Figure 11 shows the temporal evolution of the transient elongational viscosity

$$\frac{\bar{\eta}^{+} - 6\eta_s}{nkT\lambda} = \frac{1}{\lambda\dot{\varepsilon}} \frac{\tau_{p,xx}(t) - \tau_{p,zz}(t)}{nkT} \tag{47}$$

and of the mean square molecular extension $tr\langle H\boldsymbol{QQ}/kT\rangle$, for $\lambda\dot{\varepsilon} = 6$.

Insert Figure 11

During stress growth, the FENE results lie between those predicted by the FENE-P and FENE-L/LS closures. In fact, none of the three closures is very accurate there. While the FENE-L/LS models were excellent in transient uniaxial extension (Fig. 9), their performance in biaxial extension is clearly less satisfactory. In fact, we would expect that any closure based on the decoupling approximation (16) could not agree quantitatively with the FENE model in the stress growth phase for *both* uniaxial and biaxial extensions. At steady-state, the FENE-P closure is the more accurate of the three, for the same reason as discussed in uniaxial extension. Finally, all closures yield identical results in the relaxation phase.

Insert Figure 12

As seen in Fig. 12, hysteretic behaviour is obtained in this flow experiment as well. The FENE-L/LS closures do reproduce the hysteretic behaviour of the FENE model qualitatively. In comparison with uniaxial extension, they slightly overpredict the FENE hysteresis curve during the growth phase for values of mean square molecular extension above $b/2$. This in fact is related to the speed of growth of stress and molecular extension when reaching the steady-state (compare Fig. 9 and Fig. 11): overprediction is equivalent to slower growth. Comparing with Fig. 10, we observe that the shape of the hysteresis curves in uniaxial and biaxial extensions are almost identical for the FENE-L/LS closures, while it does change somewhat for the actual FENE kinetic theory. This is again due, we believe, to the decoupling approximation (16). Finally, we note that the FENE-P closure is of course unable to show hysteretic behaviour.

8 Conclusions

The FENE-L closure approximation to the kinetic theory of finitely extensible dumbbells, introduced in [1] for one-dimensional flows, has been extended in the present paper to general, three-dimensional flows kinematics. A simplified version of the theory, referred to as the FENE-LS model, has also been proposed. The reported simulations for steady and transient rheometrical flows confirm the conclusions drawn in [1] regarding the superiority of the FENE-L constitutive equation with respect to the classical FENE-P closure in describing the response of the FENE kinetic theory, both in shear and elongation. In particular, the FENE-L model is able to reproduce hysteretic behaviour in strong flows involving stress growth and subsequent relaxation, which is out of reach for a single-mode FENE-P equation. Finally, the simplified FENE-LS closure behaves similarly to its FENE-L parent, while being somewhat easier to handle numerically.

As already noted in [1], we feel that the development of even more accurate (and thus more complex) closure approximations is not warranted in this particular context. Consideration of flows in complex geometries is a more useful next step. To this

end, we have recently implemented the FENE-LS constitutive equation in a complex flow solver based upon the Adaptive Lagrangian Particle Method (ALPM) devised by Gallez *et al.* [8]. Since ALPM can also handle the actual FENE kinetic theory (i.e. without closure, but at a greater cost, obviously), additional insight should be gained as to the usefulness of the proposed new closures.

Acknowledgments

This work is supported by the ARC 97/02–210 project, Communauté Française de Belgique. The work of V. Legat is supported by the Belgian Fonds National de la Recherche Scientifique (FNRS).

References

[1] G. Lielens, P. Halin, I. Jaumain, R. Keunings, and V. Legat. New closure approximations for the kinetic theory of finitely extensible dumbbells. *J. Non-Newtonian Fluid Mech.*, 76:249–279, 1998.

[2] R.B. Bird, C.F. Curtiss, R.C. Armstrong, and O. Hassager. *Dynamics of Polymeric Liquids, Vol.2, Kinetic theory*. Wiley-Interscience, New York, 2nd edition 1987.

[3] R. Keunings. On the Peterlin approximation for finitely extensible dumbbells. *J. Non-Newtonian Fluid Mech.*, 68:85–100, 1997.

[4] R. Sizaire, G. Lielens, I. Jaumain, R. Keunings, and V. Legat. On the hysteretic behaviour of dilute polymer solutions in relaxation following extensional flow. *J. Non-Newtonian Fluid Mech.*, 82:233–253, 1999.

[5] M. Herrchen and H.C. Öttinger. A detailed comparison of various FENE dumbbell models. *J. Non-Newtonian Fluid Mech.*, 68:17–42, 1997.

[6] R.I. Tanner. Stresses in dilute solutions of bead-nonlinear-spring macromolecules. II. Unsteady flows and approximate constitutive relations. *Trans. Soc. Rheol.*, 19:37–65, 1975.

[7] H.C. Öttinger. *Stochastic Processes in Polymeric Fluids: Tools and Examples for Developing Simulation Algorithms*. Springer, Berlin, 1996.

[8] X. Gallez, P. Halin, G. Lielens, R. Keunings, and V. Legat. The Adaptive Lagrangian Particle Method for macroscopic and micro-macro computations of time-dependent viscoelastic flows. *Computer Methods in Applied Mechanics and Engineering*, accepted for publication, in press.

List of Figures

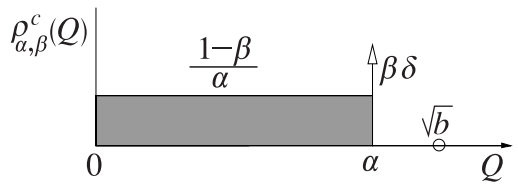

Figure 1: The FENE-L canonical distribution function.

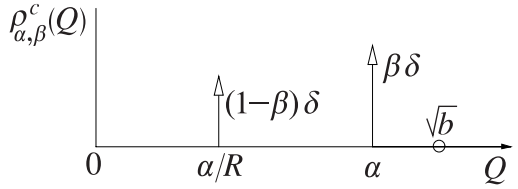

Figure 2: The FENE-LS canonical distribution function.

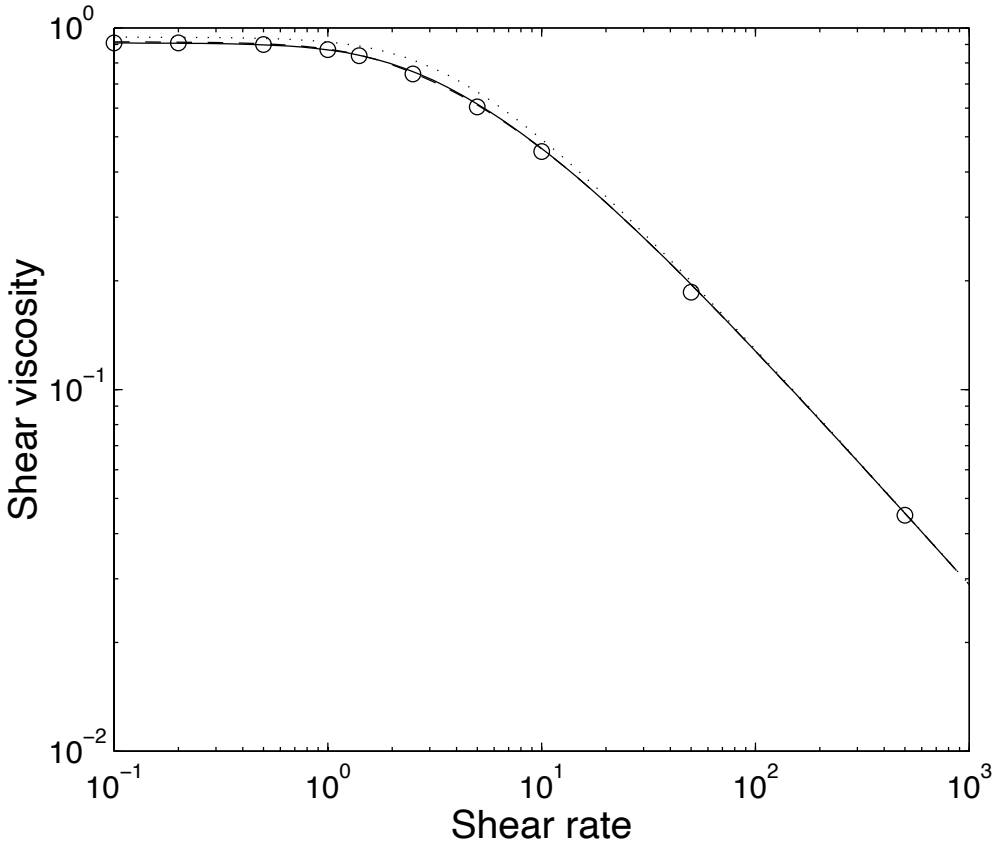

Figure 3: Dimensionless shear viscosity $(\eta - \eta_s)/nkT\lambda$ versus dimensionless shear rate $\lambda\dot{\gamma}$ for the FENE (circles), FENE-L (continuous curve), FENE-LS (dashed curve) and FENE-P (dotted curve) models with finite extensibility parameter $b = 50$. At the scale of the drawing, the FENE-L and FENE-LS results are almost identical.

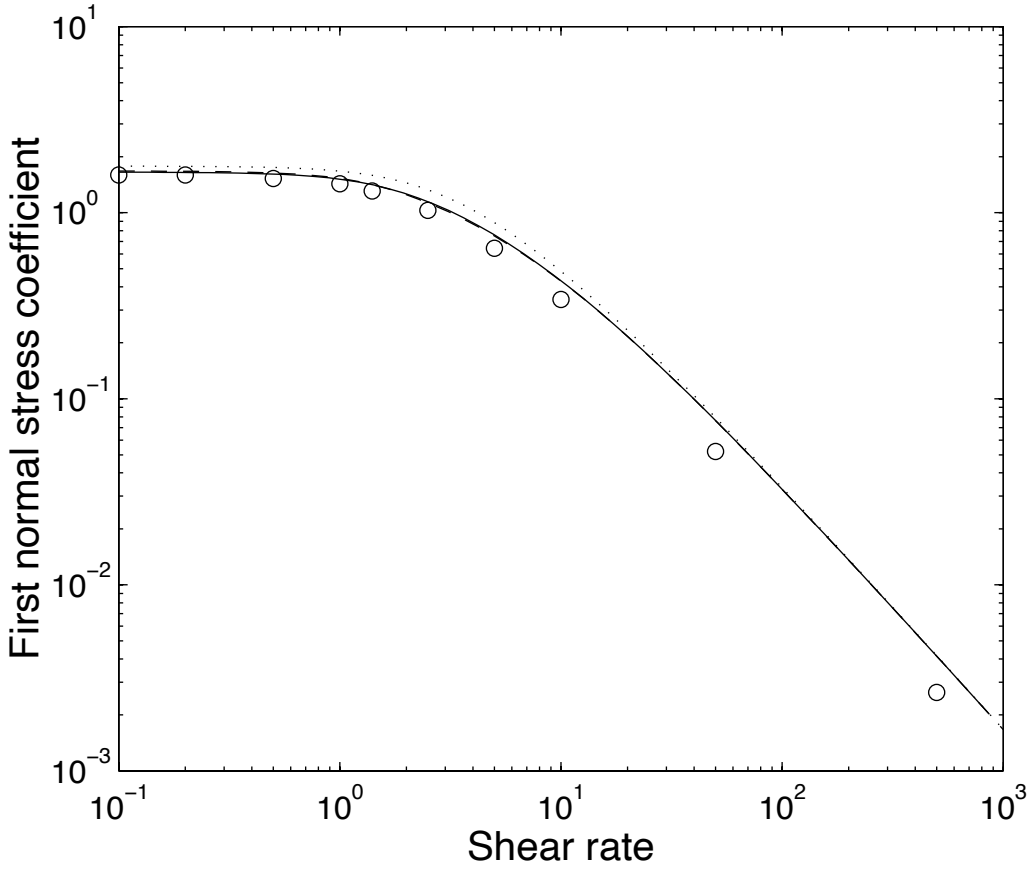

Figure 4: Dimensionless first normal stress coefficient $\psi_1/nkT\lambda^2$ versus dimensionless shear rate $\lambda\dot{\gamma}$ for the FENE (circles), FENE-L (continuous curve), FENE-LS (dashed curve) and FENE-P (dotted curve) models with finite extensibility parameter $b = 50$. At the scale of the drawing, the FENE-L and FENE-LS results are almost identical.

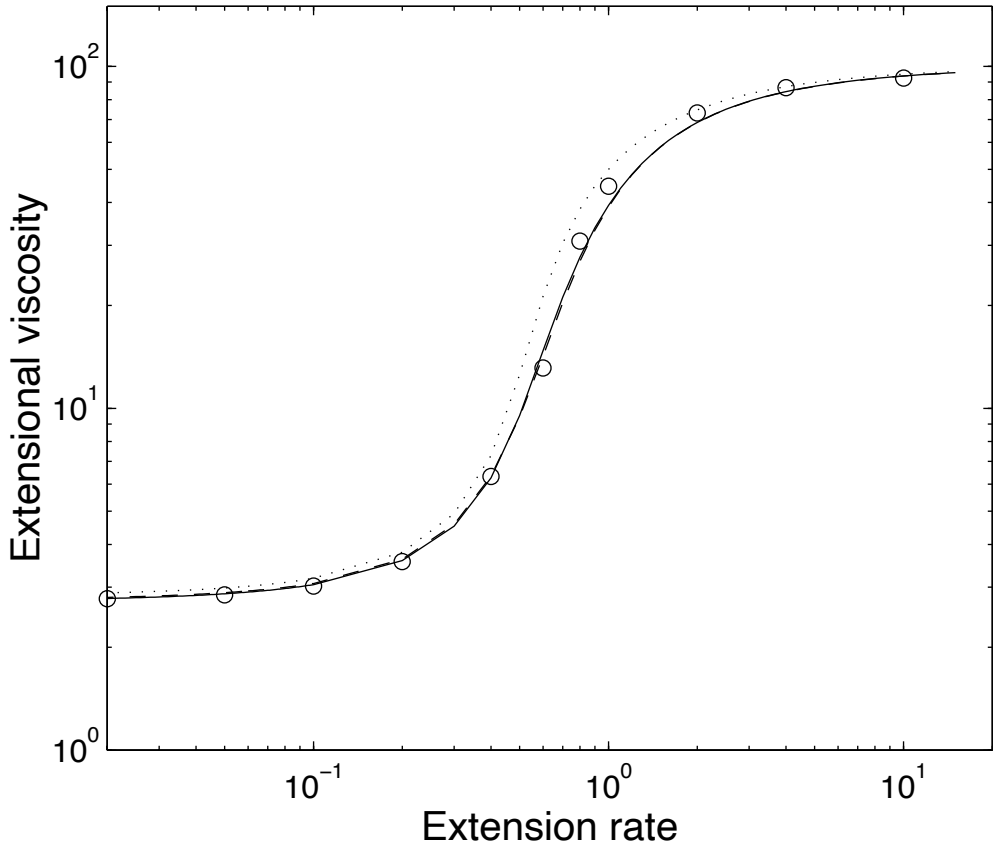

Figure 5: Dimensionless elongational viscosity $(\bar{\eta} - 3\eta_s)/nkT\lambda$ versus dimensionless extension rate $\lambda\dot{\varepsilon}$ for the FENE (circles), FENE-L (continuous curve), FENE-LS (dashed curve) and FENE-P (dotted curve) models with finite extensibility parameter $b = 50$. At the scale of the drawing, the FENE-L and FENE-LS results are almost identical.

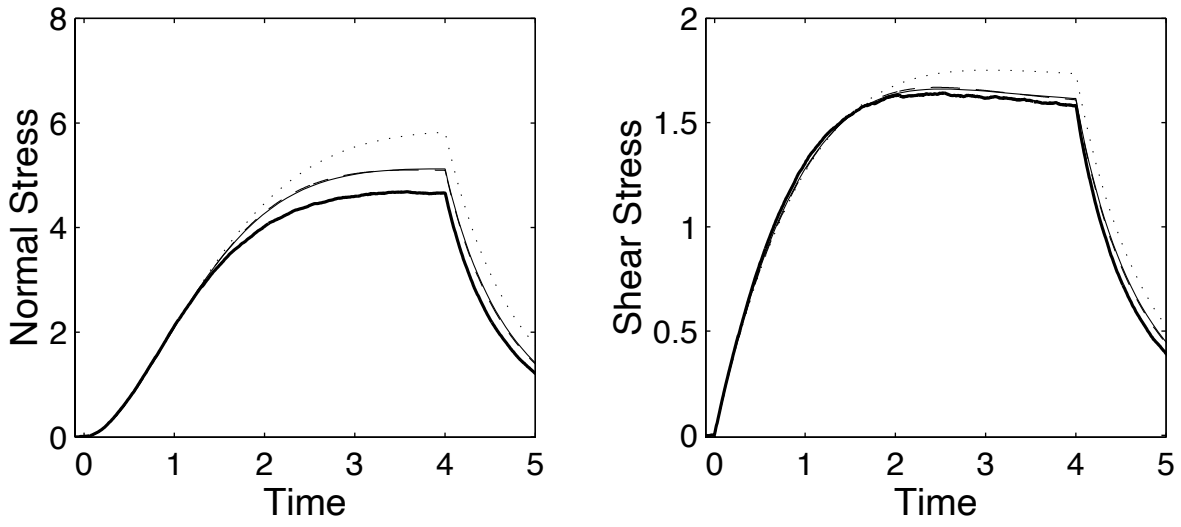

Figure 6: Start-up of simple shear ($\lambda\dot{\gamma} = 2$) followed by relaxation. Dimensionless first normal stress difference $(\tau_{p,xx} - \tau_{p,yy})/nkT\lambda$ and shear stress $\tau_{p,xy}/nkT\lambda$ versus dimensionless time t/λ for the FENE (thick curve), FENE-L (thin curve), FENE-LS (dashed curve) and FENE-P (dotted curve) models with finite extensibility parameter $b = 50$. At the scale of the drawing, the FENE-L and FENE-LS results are almost identical.

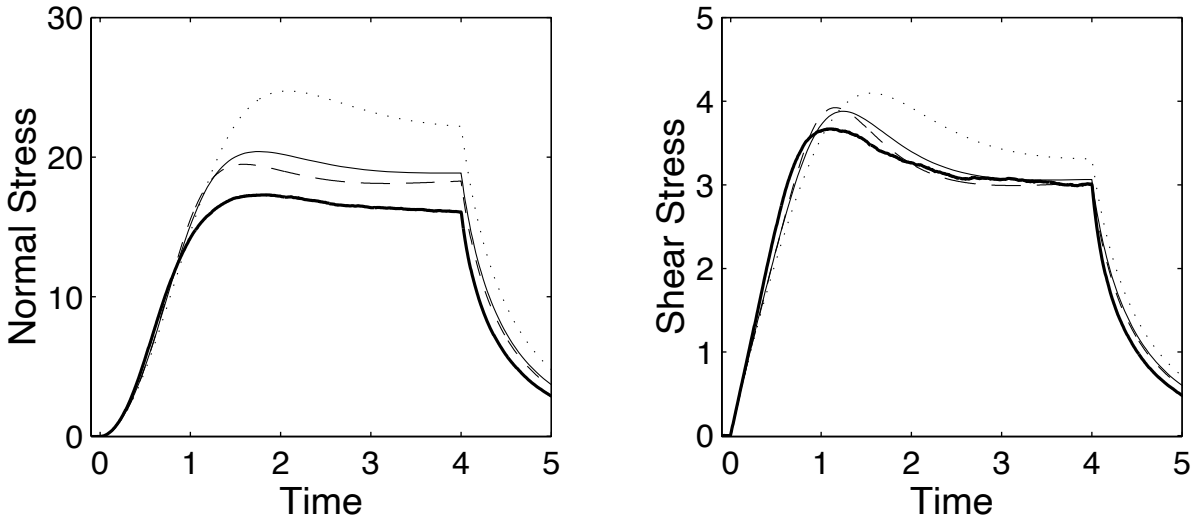

Figure 7: Start-up of simple shear ($\lambda\dot{\gamma} = 5$) followed by relaxation; cfr. Fig. 6.

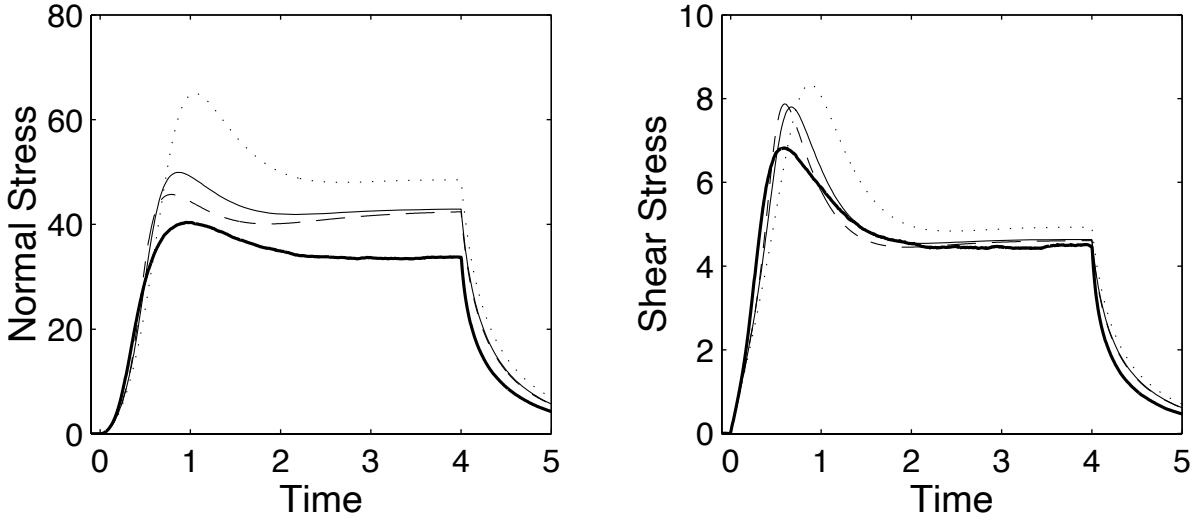

Figure 8: Start-up of simple shear ($\lambda\dot{\gamma} = 10$) followed by relaxation; cfr. Fig. 6.

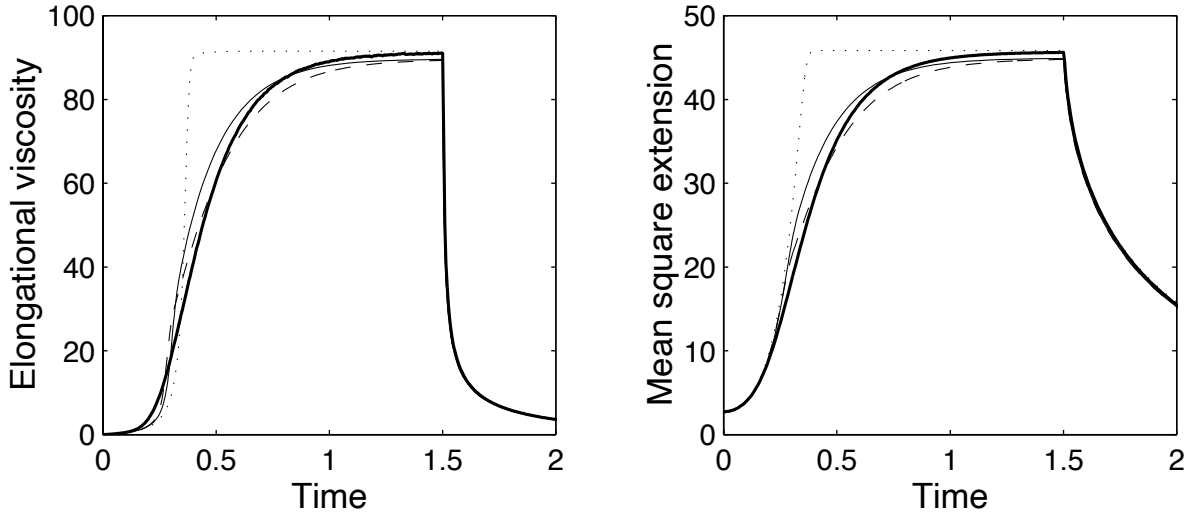

Figure 9: Start-up of uniaxial elongation ($\lambda\dot{\varepsilon} = 6$) followed by relaxation. Dimensionless transient elongational viscosity $\left(\bar{\eta}^{+} - 3\eta_s\right)/nkT\lambda$ and mean square molecular extension $tr\left\langle H\boldsymbol{QQ}/kT\right\rangle$ versus dimensionless time t/λ for the FENE (thick curve), FENE-L (thin curve), FENE-LS (dashed curve) and FENE-P (dotted curve) models with finite extensibility parameter $b = 50$.

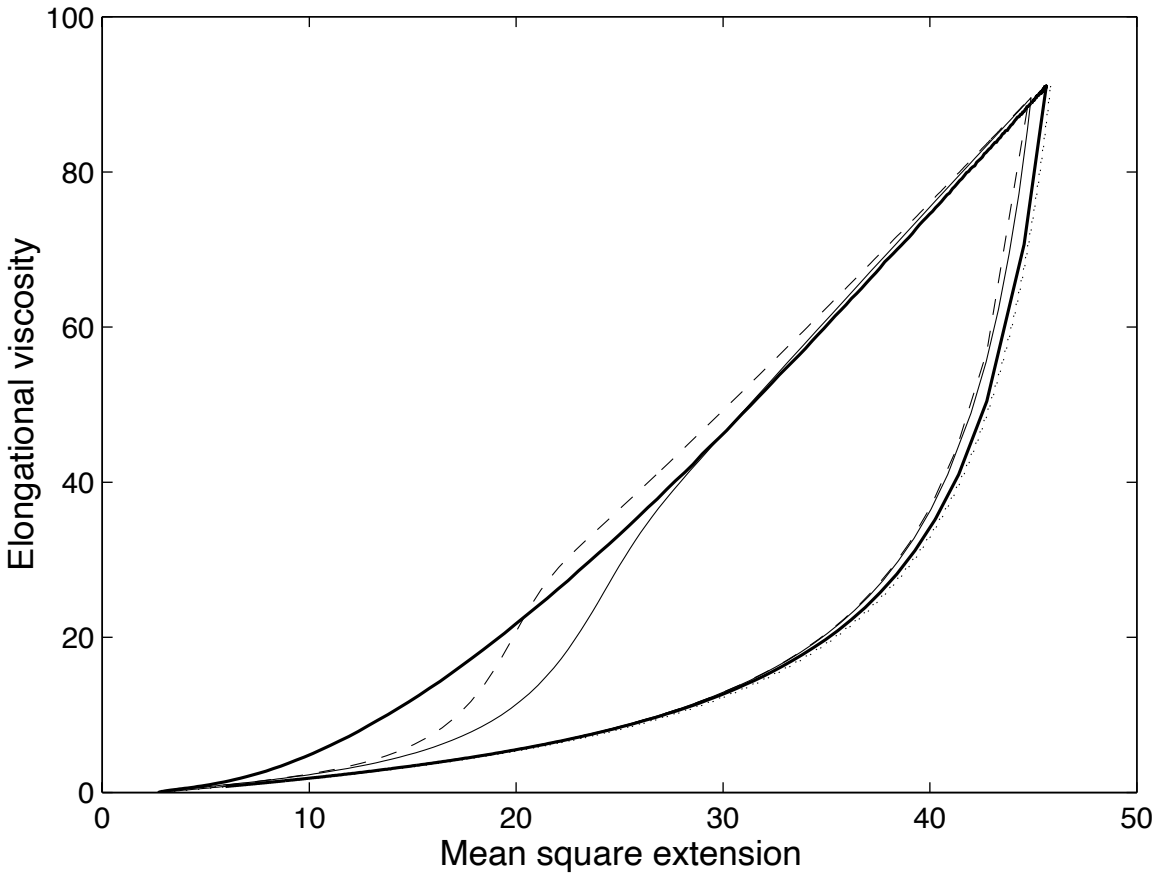

Figure 10: Start-up of uniaxial elongation ($\lambda\dot{\varepsilon} = 6$) followed by relaxation. Dimensionless transient elongational viscosity $\left(\bar{\eta}^{+} - 3\eta_s\right)/nkT\lambda$ versus mean square molecular extension $tr\left\langle H\boldsymbol{QQ}/kT\right\rangle$ for the FENE (thick curve), FENE-L (thin curve), FENE-LS (dashed curve) and FENE-P (dotted curve) models with finite extensibility parameter $b = 50$. The FENE, FENE-L and FENE-LS hysteresis curves are traversed clockwise.

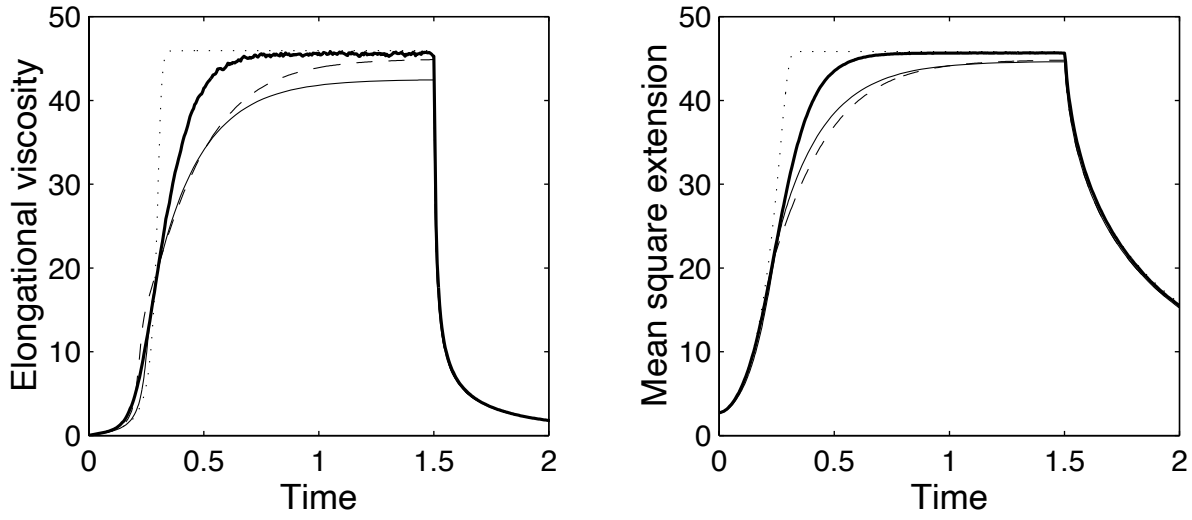

Figure 11: Start-up of biaxial elongation ($\lambda\dot{\varepsilon} = 6$) followed by relaxation. Dimensionless transient elongational viscosity $\left(\bar{\eta}^{+} - 6\eta_s\right)/nkT\lambda$ and mean square molecular extension $tr\left\langle H\boldsymbol{QQ}/kT\right\rangle$ versus dimensionless time t/λ for the FENE (thick curve), FENE-L (thin curve), FENE-LS (dashed curve) and FENE-P (dotted curve) models with finite extensibility parameter $b = 50$.

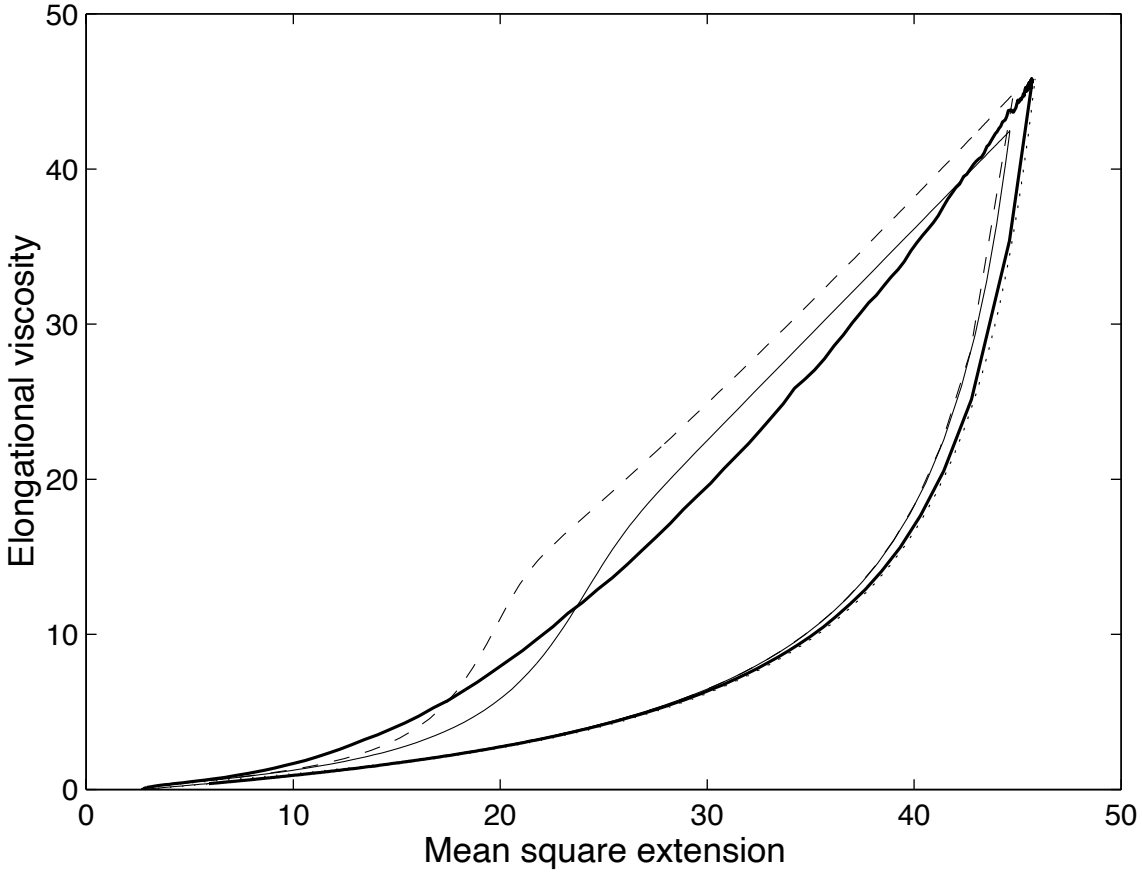

Figure 12: Start-up of biaxial elongation ($\lambda\dot{\varepsilon} = 6$) followed by relaxation. Dimensionless transient elongational viscosity $(\bar{\eta}^{+} - 6\eta_s)\,/nkT\lambda$ versus mean square molecular extension $tr\,\langle H\boldsymbol{QQ}/kT\rangle$ for the FENE (thick curve), FENE-L (thin curve), FENE-LS (dashed curve) and FENE-P (dotted curve) models with finite extensibility parameter $b = 50$. The FENE, FENE-L and FENE-LS hysteresis curves are traversed clockwise.